POSS-ENABLED MECHANICAL ENHANCEMENT FOR 3D-NANOPRINTED HIGH-ASPECT-RATIO MICROINJECTION NEEDLES

Adira Colton[1], Sunandita Sarker[1], A. Muhaymin Chowdhury[1], Prableen Chowdhary[2], Joshua A. Levy[1], Katie L. Rusland[1], Reza Ghodssi[1], Rachel Brewster[2], Kinneret Rand-Yadin[3], Ryan D. Sochol[1]

[1] University of Maryland, College Park, MD, USA

[2]University of Maryland, Baltimore County, MD, USA

[3]SeeTrue Technology, LLC., Rockville, MD, USA

ABSTRACT

Microinjection protocols that involve using a hollow, high-aspect-ratio microneedle to deliver foreign material (*e.g.*, cells, DNA, viruses, and micro/nanoparticles) into biological targets (*e.g.*, embryos, tissues, and organisms) are essential to diverse biomedical applications in both research and clinical settings. A key deficit of such protocols, however, is that standard microneedle architectures are inherently susceptible to clogging-induced failure modes, which can diminish experimental rigor and lead to failed microinjections. Additive manufacturing (or "three-dimensional (3D) printing") strategies based on "Two-Photon Direct Laser Writing (DLW)" offer a promising route to address clogging failure phenomena by rearchitecting the needle tip, yet achieving 3D-printed microneedles with the mechanical strength necessary to penetrate into biological targets (*e.g.*, embryos) has remained a critical barrier to efficacy. To overcome this barrier, here we harness a recently reported polyhedral oligomeric silsequioxane (POSS) photomaterial to DLW-print fused silica glass high-aspect-ratio microinjection needles with enhanced mechanical strength. Experimental results for POSS-based 3D-nanoprinted microneedles with inner and outer diameters of 10 μm and 15 μm, respectively, and heights ranging from 500–750 μm revealed that the needles not only enabled successful puncture and penetration into early-stage zebrafish embryos, but also significantly reduced the magnitude of undesired deformations to the embryos during needle puncture and penetration from 61.0±12.1 μm for standard glass-pulled control microneedles to 42.4±11.5 μm for the POSS-enabled 3D microneedles ($p < 0.01$). In combination, these results suggest that wide-ranging biomedical fields could benefit from the presented 3D microinjection needles.

KEYWORDS

Additive Manufacturing, Direct Laser Writing, Microinjection, 3D Printing

INTRODUCTION

Hollow glass microneedles—also referred to as "micro-capillary needles" and "micropipettes"—are critical to biomedical applications ranging from developmental biology and cancer research to stem cell therapy and *in vitro* fertilization (IVF) [1-4]. Despite their widespread use, traditional microneedles—which comprise a singular opening at the top of the tip—are inherently susceptible to clogging-associated failure phenomena, such as material from the injection target (*e.g.*, cytoplasmic material from an embryo) becoming lodged in the needle tip during puncture and penetration, thereby physically obstructing injection [5-6]. Such clogging failures are particularly problematic in cases that involve high numbers of serial microinjections (*e.g.*, in research settings) and/or high-value samples (*e.g.*, sperm/embryos for IVF) [7-9]. Previously, we reported the use of DLW for fabricating 3D micro-needle architectures, such as those with a solid fine-point tip and multiple side ports [10], which could provide a means to prevent needle clogging during insertion, but challenges stemming from microneedle mechanics remain a key bottleneck. For example, zebrafish embryos—one of the most common embryos in bio-medical research—necessitate microinjection needles with outer diameters (ODs) ≤ 15 μm to prevent catastrophic injury to the embryo, yet heights ≥ 500 μm to reach the target yolk [11-12]; however, DLW-printed needles comprising standard photomaterials along with such high-aspect-ratio architectures lack the mechanical strength required to effectively penetrate into zebrafish embryos. Although the overall geometry of the needle cannot be modified to enhance rigidity (*e.g.*, increasing the OD or decreasing the height), a DLW-compatible POSS-based photomaterial reported recently by Bauer *et al*. [13] could offer a new materials-based pathway to address the aforementioned mechanical challenges. Thus, here we investigate the potential for a POSS-based DLW-printing strategy to facilitate 3D amorphous fused silica glass microneedles with mechanical properties that are sufficient for puncturing and penetrating into early-stage zebrafish embryos (**Fig. 1**).

CONCEPT

The POSS-based 3D microneedle fabrication process includes four main steps and is based on our previously reported "*ex situ* DLW (*es*DLW)" approach for printing 3D microfluidic structures

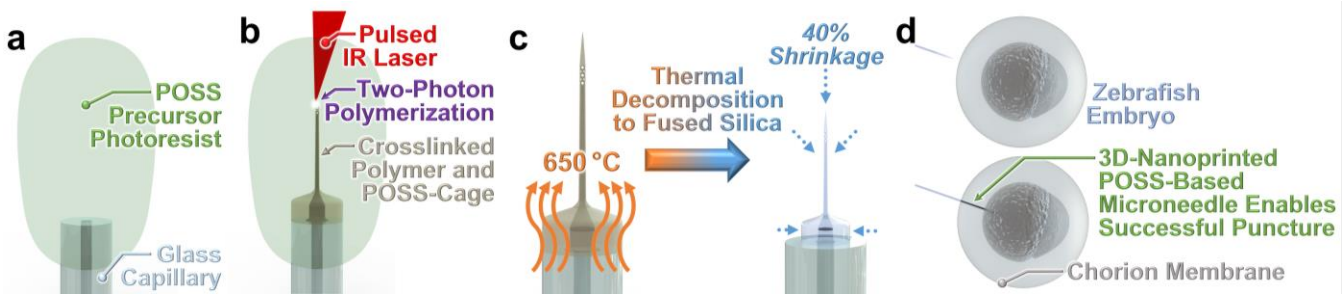

Figure 1. *Conceptual overview of the polyhedral oligomeric silsequioxane (POSS)-based "Two-Photon Direct Laser Writing (DLW)" strategy for additively manufacturing fused silica glass microneedles with the mechanical strength required for embryo microinjections.* ***(a)*** *POSS photomaterial deposited atop a glass capillary.* ***(b)*** *3D nanoprinting of the microneedle directly atop the capillary via "ex situ DLW (esDLW)".* ***(c)*** *Thermal post-processing to achieve amorphous fused silica glass microneedle.* ***(d)*** *Example application in which the resulting mechanically robust microneedle is used to puncture and penetrate into a zebrafish embryo (through the tough chorion membrane).*

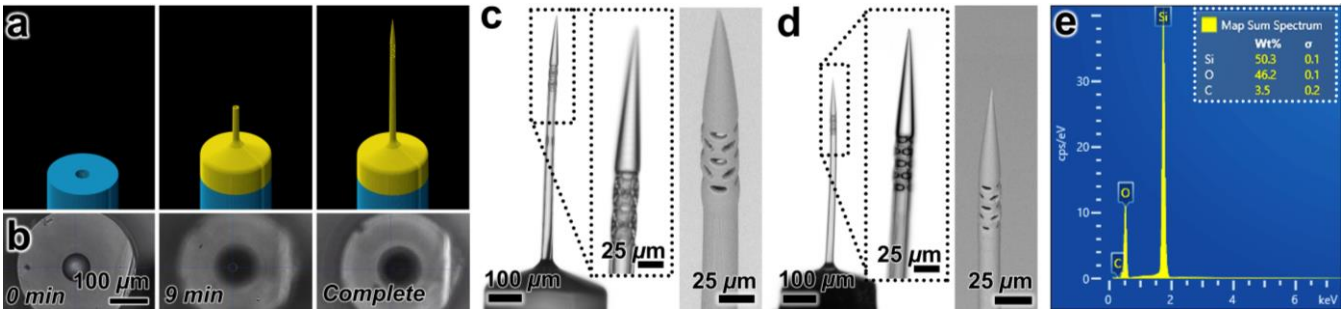

Figure 2. *Fabrication results.* ***(a, b)*** *Computer-aided manufacturing (CAM) simulations* ***(a)*** *and corresponding micrographs* ***(b)*** *of the esDLW process for 3D nanoprinting a POSS-based microneedle atop a glass capillary.* ***(c,d)*** *Brightfield (left) and SEM (right) micrographs of 3D-nanoprinted POSS-based microneedles* ***(c)*** *before, and* ***(d)*** *after the thermal post-processing protocol to achieve amorphous fused silica glass microneedles.* ***(e)*** *Energy Dispersive Spectroscopy (EDS) analysis results for the final microneedle material.*

directly atop meso/macroscale fluidic components [14-17]. First, POSS photomaterial is deposited onto an open end of a glass capillary (**Fig. 1a**). Second, a femtosecond infrared (IR) laser is scanned in a point-by-point, layer-by-layer, routine to crosslink the polymer and POSS-cage *via* two-photon (or multi-photon) polymerization phenomena (**Fig. 1b**). After completion of the *es*DLW 3D printing process, the print is developed to remove any residual POSS photomaterial. Lastly, the microneedle-capillary assembly is thermally processed to facilitate decomposition of the polymeric component, which also leads to isotropic shrinkage of the printed microneedle structure (**Fig. 1c**). Thereafter, the resulting amorphous fused silica glass microneedle can be used to puncture and penetrate through the stiff chorion membrane into zebrafish embryos (**Fig. 1d**) for microinjection applications.

MATERIAL AND METHODS

POSS-Based *es*DLW Fabrication of 3D Microinjection Needles

The POSS photoresist was prepared as described by Bauer *et al*. [13], which involved combining three components: (*i*) 89 wt% acrylic polyoctahedral silsesquioxanes (MA0736, Hybrid Plastics), (*ii*) 9 wt% ethoxylated (6) trimethylolpropane triacrylate (SR499, Sartomer), and (*iii*) 2 wt% 2-benzyl-2dimethylamino-4'-morpholinobutyrophenone (Irgacure 369, CIBA Specialty Chemicals). For the glass capillary base, amber fused silica polyimide-coated tubes (Molex LLC, Lisle, IL, USA) with an inner diameter (ID) of 75 μm and OD of 360 μm were: (*i*) cut to a length of 2 cm, (*ii*) baked at 600 °C for 1 hr (to remove the polyimide coating, which can cause burning during the DLW printing process), (*iii*) O_2 plasma etched for 30 min in a plasma cleaner (PIE Scientific), (*iv*) immersed in a silanization solution of 0.5% v/v 3-(trimethoxysily)propyl methacrylate (Sigma-Aldrich) in ethanol for 30 min, and then (*v*) rinsed with acetone and water. The glass capillaries were placed in custom holders and loaded into the DLW 3D printer (Nanoscribe GT2, Nanoscribe GmbH & Co. KG). Several drops of the POSS photomaterial were deposited on both the capillary and objective lens.

The laser writing path was generated by creating a 3D model of the microneedle in SolidWorks (Dassault Systèmes) computer-aided design (CAD) software, exporting the model as an STL file, and then importing the STL file into DeScribe (Nanoscribe) computer-aided manufacturing (CAM) software for slicing. The *es*DLW process was performed using the "Dip-in Laser Lithography (Dill)" configuration and the 25× objective lens using the Nanoscribe GT2 printer. Following completion of the *es*DLW printing process, the microneedle-capillary assembly was removed from the holder, immersed in isopropyl alcohol (IPA) for 40 min, and then allowed to air dry. The microneedle-capillary assemblies were placed into a stainless-steel baking dish (to hold them upright throughout the bake), which were then loaded inside a Linberg Blue Split Hinge Single Zone Tube Furnace (ThermoFisher). The thermal post-processing included: (*i*) a ramp up of 1.5 °C/min from room temperature to 650 °C, (*ii*) a hold at 650 °C for 1 hr, and then (*iii*) a cool down of ≤ 2 °C/min. Following the thermal processing, a marine epoxy (Loctite HY4090, Henkel Corporation) was manually placed around the base of the microneedle and allowed to cure for 24 hrs to strengthen the microneedle-capillary interface integrity.

Optical and Material Characterization of Fabrication Results

Brightfield and scanning electron microscope (SEM) images were captured using an Axio Observer.Z1 inverted microscope (Zeiss) connected to charge-coupled device (CCD) camera (Axiocam 503 Mono, Zeiss) and a TM4000 Tabletop SEM (Hitachi), respectively. Electron Dispersive Spectroscopy (EDS) results were obtained while the microneedle was within the SEM, and results were analyzed with Aztec One EDS software (Oxford Instruments).

Microneedle Mechanical Testing with Agarose Gels *In Vitro*

To facilitate interfacing between the microneedle and the pipette holder (PLI-PH1, Harvard Apparatus), the opposing end of the capillary was inserted into a thermoplastic micropipette (5-000-2005 Wiretrol II, Drummond Scientific Company) and epoxied in place (Loctite HY 4090, Henkel Corporation). This assembly was attached to a vertical translation stage (Thorlabs) and individual microneedles were lowered continuously toward—and, if possible, into—an agarose gel (10 wt%) while monitored optically.

Microneedle Experimentation with Zebrafish Embryos *In Vivo*

Zebrafish embryos in the blastula period (approximately 4 hrs post fertilization) were cultured and placed in media in a Petri dish. The POSS-based *es*DLW-printed 3D microneedles were compared against two sets of experimental control microneedles to evaluate embryo penetration efficacy, with results quantified from videos captured during the insertion process using ImageJ software (NIH): (*i*) as-printed *es*DLW-based microneedles, which were printed with a standard commercial photopolymer and did not undergo any thermal post processing, and (*ii*) standard laboratory glass microneedles. For cases in which puncture was unsuccessful, unintended deformations of the microneedles were quantified and compared to the POSS-associated case. For cases with successful penetration, unintended deformations of the embryo membrane were quantified.

RESULTS AND DISCUSSION

POSS-Based *es*DLW Fabrication and Material Properties

CAM simulations and corresponding micrographs of the *es*DLW-printing process for the POSS-based photomaterial are

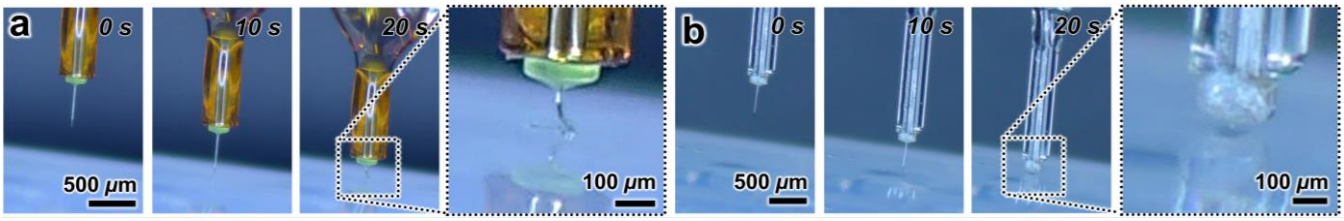

Figure 3. *Experimental results for microneedle penetration in vitro using an agarose gel (10 wt%). Sequential images from videos of representative examples for:* ***(a)*** *an as-printed experimental control 3D microneedle, and* ***(b)*** *a POSS-based esDLW-printed 3D microneedle.*

presented in **Figure 2a** and **2b**, respectively. To account for the expected 40% shrinkage [13], the as-printed microneedle designs were scaled up by 166% (*e.g.*, OD = 25 μm; ID = 16.6 μm) (**Fig. 2c**). Additionally, the base of the needle was designed with a diameter of 350 μm, which is smaller than the diameter of the uncoated capillary to prevent cracking of the base during the thermal decomposition-associated shrinkage process. Following the thermal post processing, optical characterizations revealed that the resulting microneedles resolved within 2% of the target 15 μm OD and 10 μm ID (*e.g.*, **Fig. 2d**). In addition, the results from EDS analysis corroborated the transition to amorphous fused silica, revealing material properties approximately consistent with that of a SiO_2 composition (**Fig. 2e**).

Microneedle Experimentation with Agarose Gels *In Vitro*

To initially evaluate the mechanical strength of the microneedles, we performed *in vitro* studies in which we attempted to penetrate into a 10 wt% agarose gel using POSS-based *es*DLW-printed 3D microneedles with heights of 500 μm (OD = 15 μm; ID = 10 μm) as well as an as-printed experimental control microneedle (*i.e.*, *es*DLW-printed with a standard photomaterial and without thermal post processing). In every test performed with the as-printed control microneedles, the needle consistently failed to penetrate into the agarose gel, instead revealing buckling-type mechanical failures (*e.g.*, **Fig. 3a**). In contrast, the POSS-based microneedles revealed successful puncture and penetration into the agarose gel (*e.g.*, **Fig. 3b**), providing an initial indication that the POSS-based photomaterial and post-processing steps resolve microneedles that can penetrate into targets not possible using standard as-printed photomaterials.

Microneedle Experimentation with Zebrafish Embryos *In Vivo*

To further interrogate the mechanical strength of the microneedles in cases with direct relevance to biomedical research and applications, we performed *in vivo* penetration studies with zebrafish embryos in the blastula stage, which is when the chorion membrane surrounding the embryo is at its strongest [18, 19]. Consistent with the *in vitro* experiments, the as-printed experimental control 3D microneedles were unable to penetrate into the target embryos; however, in this case, instead of buckling, the needles exhibited lateral deflections away from the direction of intended insertion (*e.g.*, **Fig. 4a**). In contrast, experiments with both the POSS-based *es*DLW-printed 3D microneedles—with heights of 750 μm, ODs of 15 μm, and IDs of 10 μm—and standard laboratory glass control microneedles revealed successful penetration into the zebrafish embryos without any signs of undesired deflections like those found for the as-printed control case (**Fig. 4a–d**).

Although both the POSS-based 3D microneedles **and** the standard laboratory glass control microneedles yielded effective embryo penetration (*e.g.*, **Fig. 4b,c**), an initial concern was that the POSS-based 3D needles might lead to higher deformations of the

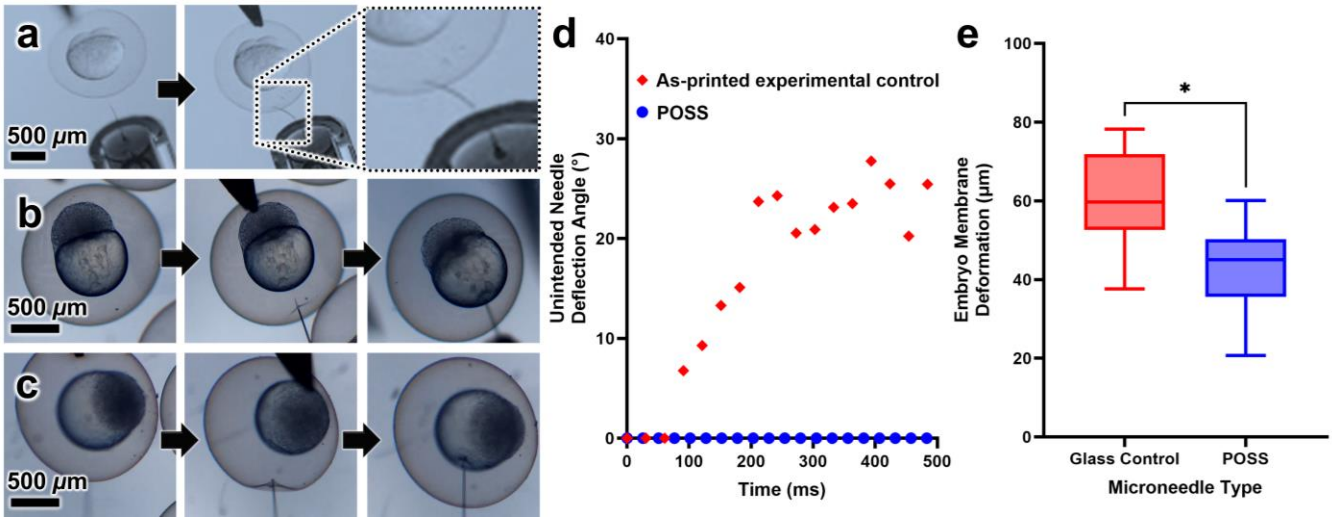

Figure 4. *Experimental results for microneedle penetration in vivo using live zebrafish embryos in the blastula period.* ***(a–c)*** *Sequential micrographs captured from representative videos of microneedle puncture and penetration attempts using:* ***(a)*** *an as-printed experimental control 3D microneedle,* ***(b)*** *a POSS-based esDLW-printed 3D microneedle, and* ***(c)*** *a standard laboratory glass control microneedle.* ***(d)*** *Quantified results for unintended lateral deflection of the microneedle (e.g., due to bending) during: (red diamonds) a failed penetration attempts with an as-printed control 3D microneedle, and (blue circles) a representative [successful] penetration case with a POSS-based esDLW-printed 3D needle.* ***(e)*** *Quantified results for undesired puncture/penetration-associated embryo membrane deformations for standard laboratory glass control needles (n = 12 embryos) versus POSS-based esDLW-printed 3D needles (n = 13 embryos). * = $p < 0.01$.*

membrane prior to puncture, which could, in turn, increase the risk of injury to the target embryo. To evaluate this potential, we quantified the magnitude of embryo membrane deformation during puncture and penetration for both cases. These results revealed a statistically significant decrease in the average membrane deformation from 61.0±12.1 μm (n = 12 embryos) for standard glass control microneedles to 42.4±11.5 μm (n = 13 embryos) for the POSS-based 3D needles ($p < 0.01$) (**Fig. 4e**), suggesting that the POSS-based *es*DLW-printed 3D microneedles could offer a new pathway to reduce damage to the embryos and/or improve ultimate viability.

CONCLUSION

Here we investigated the use of a POSS-based *es*DLW-printing and post-processing strategy to additively manufacture new classes of fused silica glass 3D microinjection needles with mechanical properties that facilitated effective puncture and penetration into live zebrafish embryos. Furthermore, because the *in vivo* embryo experiments also revealed that the presented POSS-based 3D microneedles with heights of 750 μm, ODs of 15 μm, and IDs of 10 μm led to a statistically significant reduction in the magnitude of embryo membrane deformation during puncture and penetration compared to standard laboratory glass microneedles, future efforts should focus on investigating the potential that such microneedles could mitigate pervasive microinjection-associated failure modes stemming from needle-induced injury to biological targets (*e.g.*, embryos, cells, and tissues). To our knowledge, this work marks the first demonstration of a 3D-printed hollow microneedle successfully puncturing the chorion membrane of a zebrafish embryo while also maintaining the high-aspect-ratio geometric requirements (*i.e.*, height ≥ 500 μm, OD ≤ 15 μm) for biomedical application relevance. Consequently, the strategy and results reported herein could provide a critical foundation for next-generation 3D microneedles as an enabling technology for fundamental and applied biomedical fields.

ACKNOWLEDGEMENTS

We greatly appreciate the contributions of members of the Bioinspired Advanced Manufacturing (BAM) Laboratory and Terrapin Works at the University of Maryland, College Park, and the Micro/Nanofabrication Center at the Princeton Institute of Materials. This work was supported in part by U.S. National Institutes of Health (NIH) Award Numbers 1R41GM153053 and 1R41MH135827 as well as U.S. National Science Foundation (NSF) Award Number 1943356. This material is based upon work supported by the NSF Graduate Research Fellowship Program under Grant No. DGE2236417 and DGE2139757.

CONFLICT OF INTEREST

K. Rand-Yadin is Founding Director of SeeTrue Technology, LLC., which has a potential interested in commercializing the presented 3D microinjection needles.

REFERENCES

[1] K. Hamamoto *et al.*, “Dynamic interplay between noncoding enhancer transcription and gene activity in development,” *Nature Communications*, 14, 1, (2023).

[2] Q. Zhang *et al.,* “Supplementation of mitochondria from endometrial mesenchymal stem cells improves oocyte quality in aged mice,” *Cell Proliferation*, 56, 3, e13372, (2023).

[3] R. S. J. Ingrole *et al.*, “Trends of microneedle technology in the scientific literature, patents, clinical trials and internet activity,” *Biomaterials*, 267, 120491 (2021).

[4] Y. Wang *et al.*, “Intracytoplasmic sperm injection versus conventional in-vitro fertilisation for couples with infertility with non-severe male factor: a multicentre, open-label, randomised controlled trial,” *Lancet London England*, 403, 10430 (2024).

[5] M. Li *et al.*, “Methods for the generation of heritable germline mutations in the disease vector Culex quinquefasciatus using clustered regularly interspaced short palindrome repeats-associated protein 9,” I*nsect Molecular Biology*, 29, 2, (2020).

[6] A. Shakoor *et al*., “Quality and Quantity Control of Mitochondria Injection Into Single Cells With Robot-Aided Micro-Manipulation System,” *IEEE Transactions on Automation Science and Engineering*, (2023).

[7] K. S. Ghanta *et al.*, “Microinjection for precision genome editing in Caenorhabditis elegans,” *STAR Protocols*, 2, 3, (2021).

[8] M. Bui, *et al.*, "Embryo Microinjection Techniques for Efficient Site-Specific Mutagenesis in Culex quinquefasciatus". *Journal of Visual Experimentation* 159, e61375 (2020).

[9] G. Zhang *et al.*, "Zebrafish Larva Orientation and Smooth Aspiration Control for Microinjection," in *IEEE Transactions on Biomedical Engineering*, 68, 1, (2021)

[10] Z. Wen *et al.*, “3D Nanoprinted Microinjection Needles via Ex Situ Direct Laser Writing,” *Proceedings of the 25th International Conference on Miniaturized Systems for Chemical and Life Sciences* (µTAS) , (2021).

[11] C. B. Kimmel *et al.*, "Stages of embryonic development of the zebrafish." *Developmental Dynamics,* 203, 253–310 (1995).

[12] J. Van Dycke *et al.*, “Infection of zebrafish larvae with human norovirus and evaluation of the in vivo efficacy of small-molecule inhibitors,” *Nature Protocols,* 16, 4. (2021).

[13] J. Bauer *et al*., “A sinterless, low-temperature route to 3D print nanoscale optical-grade glass,” *Science*, 380, 6648, (2023).

[14] R. Acevedo *et al.*, “3d Nanoprinted External Microfluidic Structures Via Ex Situ Direct Laser Writing,” in *2021 IEEE 34th International Conference on Micro Electro Mechanical Systems (MEMS),* (2021), pp. 10–13.

[15] S. Sarker *et al*., “3D-Printed Microinjection Needle Arrays via a Hybrid DLP-Direct Laser Writing Strategy,” *Advanced Material Technologies*, (2023).

[16] O. M. Young *et al*., “3D Microprinting of Multi-Actuator Soft Robots onto 3D-Printed Microfluidic Devices via Ex Situ Direct Laser Writing,” *20th Solid-State Sensor and Actuators Workshop* Hilton Head Island SC USA (2022), pp. 332–335.

[17] A. Colton *et al.*, “Toward “S”-Shaped 3D-Printed Soft Robotic Guidewires for Pediatric Patent Ductus Arteriosus Endovascular Interventions” in *2024 IEEE International Conference on Soft Robotics (RoboSoft), San Diego, USA, (2024).*

[18] S. Vergote *et al.*, “Preterm membranes are mechanically more resistant than term membranes,” *Prenatal Diagnosis*, 44, 3. (2024).

[19] M. Pérez-Atehortúa *et al.*, “Chorion in fish: Synthesis, functions and factors associated with its malformations,” *Aquaculture Reports*, 30, (2023).

CONTACT

*A. Colton; tel: +1-301-405-6928; acolton1@umd.edu